Growth and Dissolution of Potash Alum Crystals in the Subsieve Size Range

Overall growth and dissolution rates of potash alum crystals have been measured over the size range 3 to 70 μm. The derived surface integration growth kinetics, which are found to be linear with respect to supersaturation and strongly size dependent, are evaluated in terms of the step model of crystal growth. The results emphasize the importance of independently measuring growth kinetics before secondary nucleation kinetics can be calculated from MSMPR experiments.

JOHN GARSIDE

and

SLOBODAN J. JANČIĆ

Department of Chemical Engineering
University College London
Torrington Place, London WC1E 7JE, U.K.

SCOPE

Determination of crystal growth and nucleation kinetics from the crystal size distribution (CSD) in continuous crystallizers is now a well-established technique. The use of Coulter counters to measure these size distributions in the range between about 1 and 50 μm has, however, posed new problems in interpretation. It is clear that secondary nucleation, the dominant mode of nucleation in industrial crystallizers, results in new crystals being produced over a range of sizes that extends up to perhaps 15 μm. Because nuclei are produced at a size other than zero, the CSD can no longer be used to calculate nucleation rates unless the variation of growth rate with crystal size is independently known. To overcome this problem, previous workers (Randolph and Cise, 1972; Youngquist and Randolph, 1972) have assumed either that all nuclei are produced at zero size, or that the growth rate of crystals for the size range into which nuclei are produced is zero.

It is the objective of the present study to directly measure crystal growth kinetics in the small size range. The results of such measurements may then be combined with CSDs obtained from continuous crystallizers to determine true secondary nucleation kinetics. Further, growth kinetics obtained for small crystals provide a comparison with similar kinetics for much larger crystals, so giving an insight into the effect of crystal size on the mechanism of crystal growth.

CONCLUSIONS AND SIGNIFICANCE

The surface integration kinetics of potash alum crystals in the size range between about 3 and 70 μm are shown to be linear with respect to supersaturation and, at a given supersaturation, to increase markedly with size; for example, the growth rate of 70 μm crystals is some twenty times that of 3 μm crystals, about half the increase occurring between 3 and 15 μm. Previously published results (Garside et al., 1975) for much larger (> 500 μm) crystals show the same trend and are consistent with the present work.

These observations can be explained by supposing that for larger crystals increasingly energetic crystal collisions combined with mechanical stresses and the incorporation of impurity atoms into the crystal lattice cause the dislocation density to increase. This, in turn, strengthens the step source on the crystal surface and so increases the growth rate.

On the basis of the results, overall growth kinetics in a typical laboratory crystallizer are estimated. The resulting growth rates are strongly size dependent for sizes less than about 100 μm but become almost independent of size for crystals larger than about 500 μm. These results emphasize the importance of independently measuring growth kinetics before accurate secondary nucleation rates can be obtained from steady state crystal size distributions in MSMPR crystallizers.

Crystal growth kinetics covering a wide range of experimental conditions have been published for many systems. In particular, the effect of crystal size on growth rate has been reported by, for example, Mullin and Garside (1967), Garside et al. (1974), and Phillips and Epstein (1974). All these studies have covered the size range between about 0.3 and 4 mm. While such measurements give important information concerning the mechanism of crystal growth, the size range of crystals encountered in industrial crystallizers extends at least two orders of magnitude below this range, that is, down to about 1 μm. Some authors have suggested that at these small sizes the crystal growth rate is very small (Randolph and Cise, 1972) or that many very small crystals do not grow (Bujac, 1976).

From a knowledge of the steady state crystal size distribution, crystal growth rates can be obtained for the entire size spectrum present in continuous MSMPR crystallizers, provided that the size ranges under investigation are populated entirely by growth. There is ample evidence, however, that direct birth of secondary nuclei contributes significantly to the observed crystal population for sizes less than about 15 μm. It is not possible to determine two size dependent functions, the birth rate $B(L)$ and the growth rate $G(L)$, from the measurement of only one size dependent variable, the population density $n(L)$. Randolph and his co-workers (Youngquist and Randolph, 1972; Randolph and Cise, 1972) overcame this problem by making one of two limiting assumptions. They either assumed that all nuclei were produced at zero size, that is,

Correspondence concerning this paper should be addressed to John Garside.

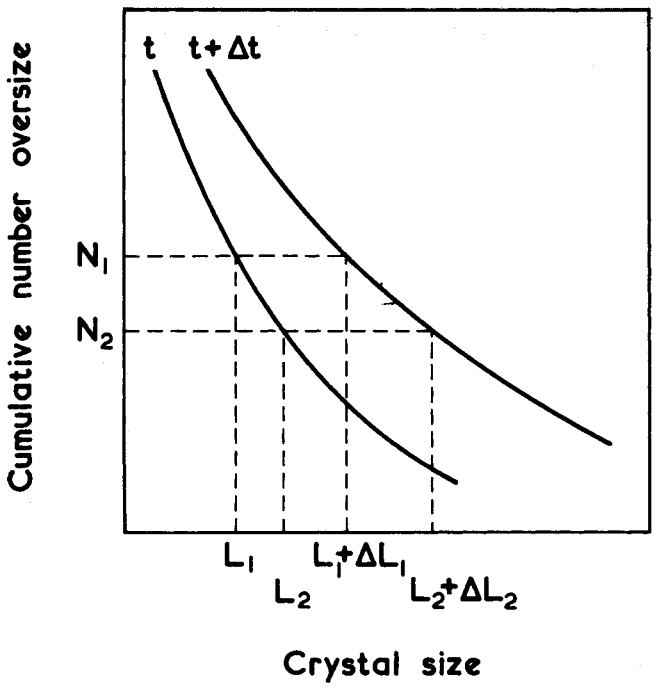

Fig. 1. Calculation of growth rates from transient size distributions.

$B(L) = 0$ for $L > 0$, or they assumed that population changes due to growth were negligible over the size range into which secondary nuclei were born, that is, $G(L) = 0$ for $L < L_{max}$, L_{max} being the maximum size at which secondary nuclei were produced.

One objective of the study reported here was to avoid the necessity for making either of these assumptions by independently measuring crystal growth rates in the subsieve size range. Secondary nucleation kinetics derived by combining the growth rates reported in this paper with the results of MSMPR experiments will be presented in a further communication.

A second objective of the present work was to compare growth rates in the subsieve size range with previous results for much larger crystals. Size dependent surface integration kinetics have been measured for a number of systems, and the present work extends such measurements down to about 3 μm.

The potash alum-water system was chosen for the present study, since the growth characteristics of larger crystals are well defined (Garside et al., 1975), and MSMPR experiments combined with steady state crystal size distribution measurements down to about 5 μm have been successfully performed (Jancic and Garside, 1975, 1976).

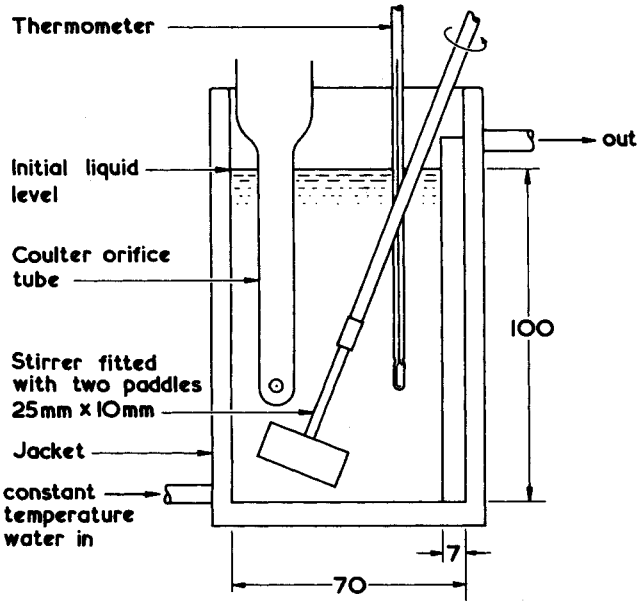

Fig. 2. Vessel used for growth and dissolution experiments (all dimensions in millimeters).

DETERMINATION OF GROWTH AND DISSOLUTION RATES

The experimental technique makes use of a Coulter counter to follow changes in the size distribution of small crystals growing or dissolving under well-defined conditions.

Misra and White (1971) have previously reported a somewhat similar technique by which growth rates of aluminum trihydroxide in caustic aluminate solutions were measured. The very slow growth rates observed with this latter system allowed growth runs to last up to 3 days. Furthermore, prior to size analysis, the trihydroxide crystals were removed from the crystallizer, separated from solution, dried, and dispersed in a suitable electrolyte before being introduced into a Coulter counter sampling beaker. In the present work, seed crystals were allowed to grow in the Coulter counter sampling beaker so that the size analysis was performed in situ without the necessity of sampling and subsequent handling of the crystal sample.

Calculation of crystal growth and dissolution rates is facilitated if the crystal size distribution is represented in terms of cumulative number oversize, since the cumulative numbers in a distribution undergoing transients caused solely by crystal growth are invariant with time. The procedure used to calculate linear growth or dissolution rates can be described with reference to Figure 1 in which two arbitrary transients of the cumulative number oversize distribution are presented. At time t, the size range L_1 to L_2 contains $(N_1 - N_2)$ crystals. As growth proceeds, the crystals pass through size groups at their respective growth rates so that $(N_1 - N_2)$ crystals are confined to the size range between $L_1 + \Delta L_1$ and $L_2 + \Delta L_2$ at time $t + \Delta t$. The average growth rate for the group of $(N_1 - N_2)$ crystals is

$$\overline{G}(L,t) = \frac{\dfrac{L_1 + \Delta L_1 + L_2 + \Delta L_2}{2} - \dfrac{L_1 + L_2}{2}}{(t + \Delta t) - t} = \frac{\Delta L_1 + \Delta L_2}{2\Delta t} \tag{1}$$

In the limit as $L_2 \to L_1$, and assuming no dispersion in crystal growth, $\Delta L_2 \to \Delta L_1$ and $N_2 \to N_1$, the number of crystals with size greater than L_1. Equation (1) then becomes

$$\overline{G}(L,t)_{L+\frac{\Delta L}{2}} = \frac{\Delta L}{\Delta t} \tag{2}$$

Thus, crystal growth rates can be evaluated from the displacement, ΔL, between two transients at a constant value of the cumulative number oversize distribution as shown in Figure 1.

This method is satisfactory so long as the total number of crystals in the distribution remains constant. If the total number of crystals increases (owing, for example, to secondary nucleation) or decreases (owing to dissolution of the very smallest crystals), then the above method may still be used provided that the size ranges into which secondary nuclei are born, or from which crystals disappear, are not considered.

EXPERIMENTAL TECHNIQUE

A model TA Coulter counter was used in the present work. This instrument presents the size analysis in terms of a differential or cumulative mass distribution together with the total number of particles counted in the complete size analysis. If successive size distributions measured during a growth or dissolution run are always made by using the same sample volume, an immediate indication of the occurrence of secondary nucleation or total dissolution of crystals from the distribution is obtained.

Growth and dissolution rates of potash alum crystals were measured in the agitated vessel illustrated in Figure 2. This had a capacity of 250 ml and was jacketed, the solution temperature being maintained at 30° ± 0.05°C by circulating thermostatically controlled water through the jacket. The crystals were kept suspended by a stirrer fitted with two flat paddles mounted at right angles, one above the other. This was rotated at a fixed speed (3.3 rev/s) for all runs. Vortex and bubble formation were reduced by baffles.

The Coulter counter sampling probe was mounted directly in the vessel, and orifice tubes having diameters of 70, 100, and 280 μm were used as appropriate to the size of the crystal seeds. Very high levels of background noise were initially obtained, but these were drastically reduced to acceptable levels by earthing the inlet and outlet circulating water lines and by thorough electrical shielding of the growth vessel and instrument glassware.

Solutions of the desired concentration were prepared from recrystallized potash alum and deionized water. In order to ensure that the background count was as low as possible, the solution, at a temperature above the saturation point, was filtered through an 0.45 μm membrane filter just prior to the start of a run. Solution concentration measurements were made by determining the solution density with a pyknometer. From a standard procedure (ASTM, 1963), the repeatability of the density measurements was $\pm$ 2 $\times$ 10^{-5} g/cm^3. After inaccuracies in the solubility and fluctuations in the solution temperature were allowed for, it was estimated that the 95% confidence limits of measured values of $(c - c^*)$ were equivalent to about 30% at $(c - c^*) = 10^{-3}$ kg hydrate/kg solution and about 5% at $(c - c^*) = 8 \times 10^{-3}$ kg hydrate/kg solution. Full details of these estimates are given elsewhere (Jancic, 1976). Since a very small mass of seed crystals ($\simeq$ 3 mg) was used in each growth and dissolution experiment, the solution supersaturation remained essentially constant throughout a run.

For experiments in which crystals larger than about 30 μm were used, seed crystals were taken from sieve cuts of dried samples obtained in a cooling MSMPR crystallizer (Jancic and Garside, 1975, Jancic, 1976). Microscopic examination showed that more than 95% of these crystals were well formed, single octahedra. For experiments with smaller crystals, seeds were obtained from one of two sources. Some seeds were produced by carefully milling larger crystals which were then separated into various size fractions by using microsieves. Other small seeds were obtained by removing a small sample of liquor from an MSMPR crystallizer and by introducing this sample into the growth vessel through a micromesh screen. Variations in the size of the mesh allowed different seed sizes to be obtained. The growth rates of crystals obtained from these two sources appeared to be identical, as will be discussed below.

After the seed crystals were introduced into the growth vessel, they were allowed to grow for about 2 min in order to heal any surface damage. An initial crystal size analysis was then performed. Each size analysis took about 10 s, and a run was continued until the total particle count

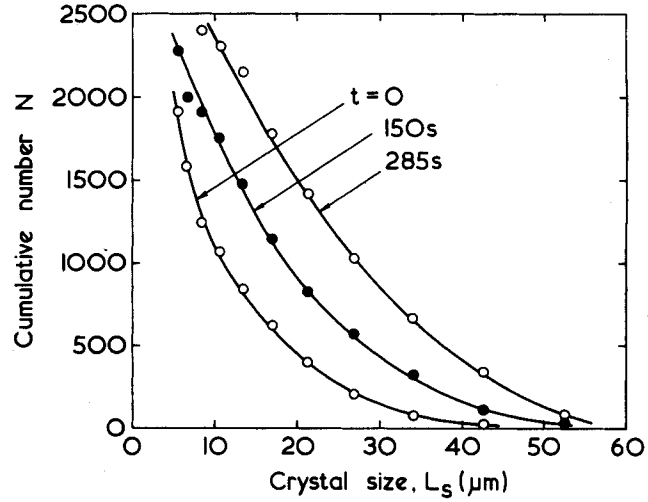

Fig. 3. Development of crystal size distribution during a growth run ($c - c^* = 0.55 \times 10^{-2}$ kg hydrate/kg solution).

indicated that significant secondary nucleation or total dissolution was occurring. Before each count was performed, it was necessary to remove any crystals that had lodged in the orifice of the sampling tube by using a very fine artist's brush. Microscopic examination of the orifice showed that this procedure ensured an unobstructed orifice throughout the duration of a count.

Figure 3 shows three successive number distributions for a typical growth run. These distributions were derived from the Coulter counter output data and are expressed in terms of L_s, the length of an edge of the potash alum octahedra. This is related to the Coulter counter channel size L_c (which represents the diameter of a sphere having the same volume as the particle being sized) by (Jancic

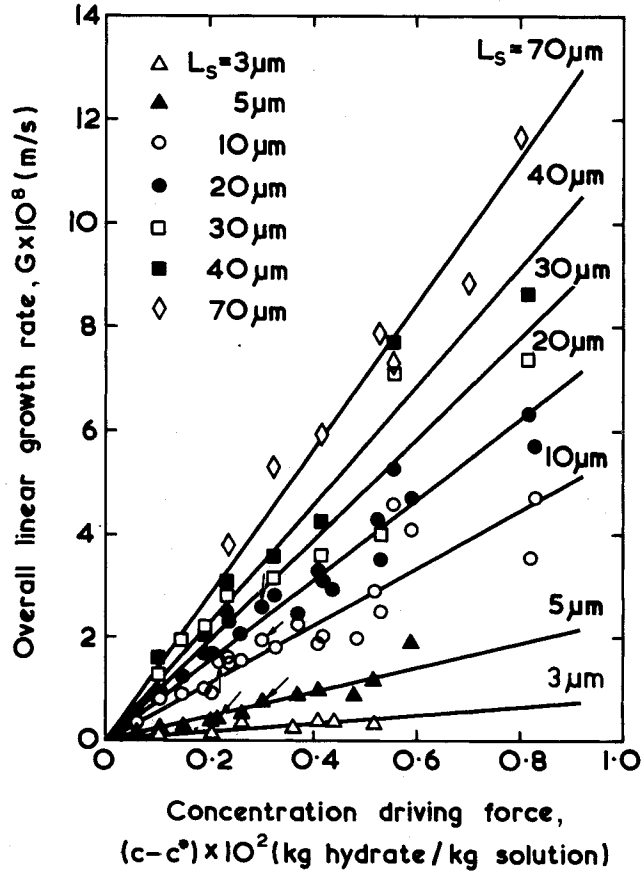

Fig. 4. Overall crystal growth kinetics at 30.0°C (arrowed points obtained from MSMPR seed crystals).

and Garside, 1975)

$$L_s = 1.036\ L_c \qquad (3)$$

Crystal growth and dissolution rates at specific sizes were calculated by using Equation (2) from plots such as that shown in Figure 3. These rates are thus expressed as the time rate of change of L_s and are represented by G and G_D for the growth and dissolution rates, respectively.

RESULTS

Overall Growth Rates

Overall crystal growth rates at 30.0°C are plotted as a function of concentration driving force $(c - c^*)$ and crystal size in Figure 4. The results obtained by using crystals taken directly from an MSMPR crystallizer are indicated, and it can be seen that these are not significantly different from the other results. Growth rate increases with both concentration driving force and crystal size, the dependence on $(c - c^*)$ being approximately first order. The overall growth rates may thus be correlated by the equation

$$G = K_G\ (c - c^*) \qquad (4)$$

where K_G is a function of crystal size. Values obtained from the best straight lines through the points in Figure 4 are shown in Table 1, together with the 95% confidence limits of the estimates.

The effect of crystal size is very pronounced, particularly for the smaller sizes investigated (below about 20 μm). For example, the growth rate at a given value of $(c - c^*)$ increases by a factor of about 20 over the size range from 3 to 70 μm, with half of this increase occurring between 3 and 15 μm. The reason for this increase will be discussed later.

A number of empirical equations have been proposed to describe the effect of crystal size on the overall growth rate. Perhaps the most satisfactory of these is the equation of Abegg, Stevens, and Larson (1968) (the ASL equation) which may be written

$$G = G_o\ (1 + \gamma L)^b \quad \text{for} \quad b < 1 \qquad (5)$$

If the growth rate of nuclei G_o is expressed as

$$G_o = K_{Go}\ (c - c^*)^g \qquad (6)$$

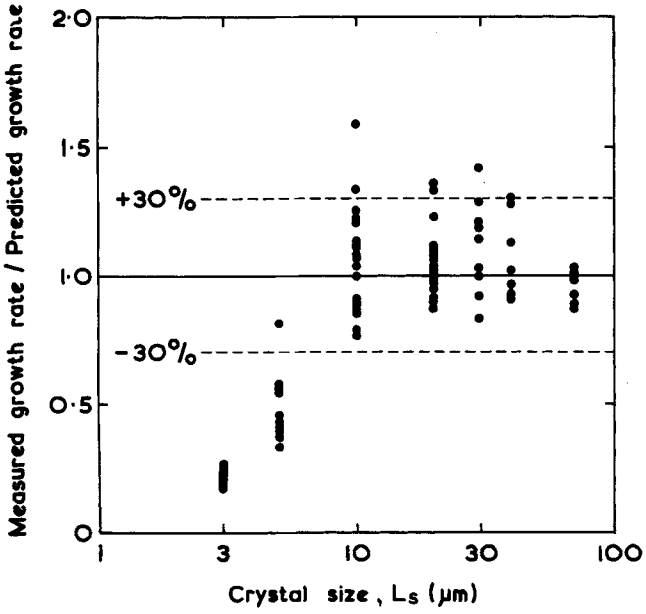

Fig. 5. Measured overall growth rates compared with those predicted from Equation (8).

Table 1. Variation of Growth and Dissolution Parameters with Crystal Size (95% Confidence Limits are Indicated in the Table)

Crystal size L_s (μm)	Overall growth rate coefficient K_G (μm/s)	Mass transfer coefficient k_d (μm/s)	Surface integration rate coefficient k_r (μm/s)
3	0.77 ± 0.08	36.3 ± 21.2	0.10 ± 0.02
5	2.37 ± 0.01	71.2 ± 23.0	0.31 ± 0.02
10	5.55 ± 0.28	16.8 ± 6.0	0.84 ± 0.10
20	7.73 ± 0.22	70.6 ± 15.8	1.06 ± 0.07
30	9.69 ± 0.65	100 ± 21	1.35 ± 0.18
40	11.4 ± 0.6	100 ± 13	1.62 ± 0.18
70	14.0 ± 0.4	74.0 ± 12.8	2.01 ± 0.19
100	—	36.1 ± 3.8	—

then the equation

$$G = K_{Go}\ (c - c^*)^g\ (1 + \gamma L)^b \qquad (7)$$

is an empirical relationship which may be used to correlate the effects of supersaturation and crystal size on growth rate.

Equation (7) was fitted to the results described above by using a nonlinear least-squares library subroutine. The resulting equation, based on 80 data points, is

$$G = 9.6 \times 10^{-8}(c - c^*)^{0.90}\ (1 + 61L)^{0.54} \qquad (8)$$

where the units of G are meters per second, of Δc are kilogram hydrate per kilogram solution, and of L are micrometers. The overall quality of the prediction of Equation (8) is illustrated in Figure 5, where the ratio of measured to predicted growth rate is plotted as a function of crystal size. The fit is satisfactory in the size range 10 to 70 μm but deteriorates rapidly for crystals smaller than 10 μm.

Dissolution Rates

Dissolution rates of small crystals were measured at 30.0°C under hydrodynamic conditions identical to those used for the growth experiments. Representative results are shown in Figure 6. The linear dissolution rates G_D were always first order with respect to concentration driving force and were about one order of magnitude higher than the corresponding growth rates.

Conventional mass transfer coefficients are related to the mass flux from the solid surface R_D and the concentration driving force (expressed in terms of a mass density) by the relation

$$R_D = k_d\ (\rho^* - \rho) \qquad (9)$$

The linear dissolution rate G_D is thus related to k_d through the equation

$$G_D = \frac{f_s}{3 f_v \rho_c} \cdot k_d\ (\rho^* - \rho) \qquad (10)$$

where f_s and f_v are the surface and volume shape factors defined by $s_c = f_s L_s^2$ and $v_c = f_v L_s^3$. For an octahedron, $f_s = 3.46$ and $f_v = 0.471$.

Experimental mass transfer coeffcients were calculated for a number of crystal sizes by using Equation (10), and these are shown in Table 1 and Figure 7. Because of the speed at which dissolution took place, the measurements involved greater experimental difficulties than the growth experiments. In particular, successive size analyses had to be made after very short intervals of time. Consequently, the dissolution results are probably less accurate than the corresponding growth rates, and this is reflected in the greater scatter of experimental points in Figures 6 and 7.

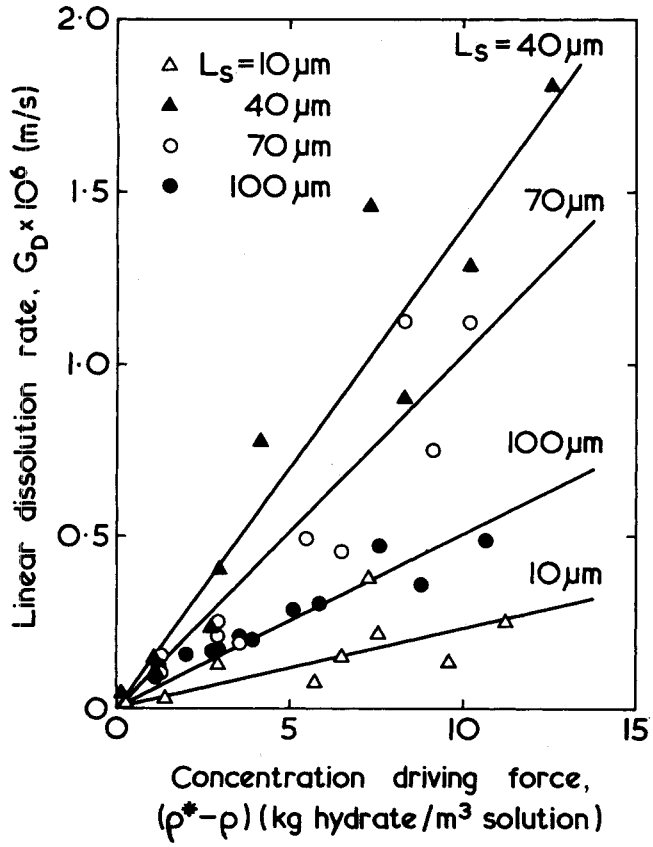

Fig. 6. Crystal dissolution kinetics at 30.0°C.

In spite of this, the trend shown in Figure 7 is reasonably clear. For crystals larger than about 30 μm, the mass transfer coefficient decreases with increasing size. Below 30 μm, however, the results suggest a decrease in k_d with decreasing size.

Prediction of solid/liquid mass transfer coefficients in agitated tanks is somewhat uncertain, since the relative velocity between the particle and fluid, and hence the Reynolds number, is difficult to evaluate. The predictions of two of the more recent correlations (those of Levins and Glastonbury, 1972, and Nienow, 1975) have been included in Figure 7, together with the curve corresponding to $Sh = 2$ which represents the limiting case for diffusion in an infinite, stagnant fluid. When using these correlations, the following conditions were observed:

1. The crystals were assumed to be spheres of diameter L_s.
2. The stirrer Reynolds number, $\rho_s d^2 N_s/\mu$, was calculated to be 2 000. The corresponding power number was estimated as 2.7 (Nienow and Miles, 1971) and hence the power dissipation per unit mass of solution, $\epsilon \simeq 7 \times 10^{-3}$ $m^2 s^{-3}$.
3. Physical properties for the potash alum/water system were obtained from the data of Mullin et al. (1965).

Results for crystals larger than about 30 μm show the same trend as predicted by all the correlations, although the present results are somewhat higher than the predicted values. In view of the possible experimental errors and the assumptions made in deriving the predicted curves, this agreement can be considered satisfactory. Measured mass transfer coefficients for crystals smaller than about 30 μm, however, do not continue to increase with decreasing size as would be expected from theoretical considerations. The data points in these small size ranges are the least accurate, since the small crystals tend to disappear quickly from the distribution. Somewhat similar results have recently been reported by Nagata and Nishikawa (1972) who dissolved copper particles in sulfuric acid and gypsum and barium sulfate in water. Their results showed that for very small particles (< 10 μm) the rapid increase in mass transfer coefficients suggested by all the correlations did not take place. It was suggested that these small particles, being smaller than the microeddies, were trapped within the eddies where viscous effects predominated. The rate controlling process then becomes the transfer of solution from the microeddies to the surrounding liquid rather than transfer from the dissolving particles to the fluid.

Surface Integration Rates

The overall crystal growth rates reported here for potash alum are about an order of magnitude smaller than the corresponding dissolution rates. The overall rates will thus differ little from the surface integration kinetics. The actual surface integration kinetics were, however, calculated by assuming that the mass transfer coefficient measured for dissolution could also be used to estimate the volume diffusion resistance present during growth. The concentration at the crystal/solution interface was thus calculated by using the procedure that has been employed previously (Garside et al., 1975).

The growth rates were correlated with the calculated supersaturation at the interface σ_i $(= (\rho_i - \rho^*)/\rho^*)$ by using the equation

$$G = k_r \sigma_i^n \qquad (11)$$

The values of n for crystals of different size varied between 0.76 and 1.16. There was no discernible trend of n with crystal size, and the standard deviations of the estimates of n were such that a value of $n = 1$ is justified for all crystal sizes. Values of k_r in the equation

$$G = k_r \sigma_i \qquad (12)$$

are shown in Table 1. As would be anticipated from the previous discussion, the surface integration kinetics are strongly size dependent.

Previous potash alum growth rates measured in a fluidized bed (Mullin and Garside, 1967) have recently been reevaluated (Garside et al., 1975). It was concluded that the surface integration kinetics, derived from overall growth rates by the procedure subsequently used in the present paper, were size dependent. The results of these

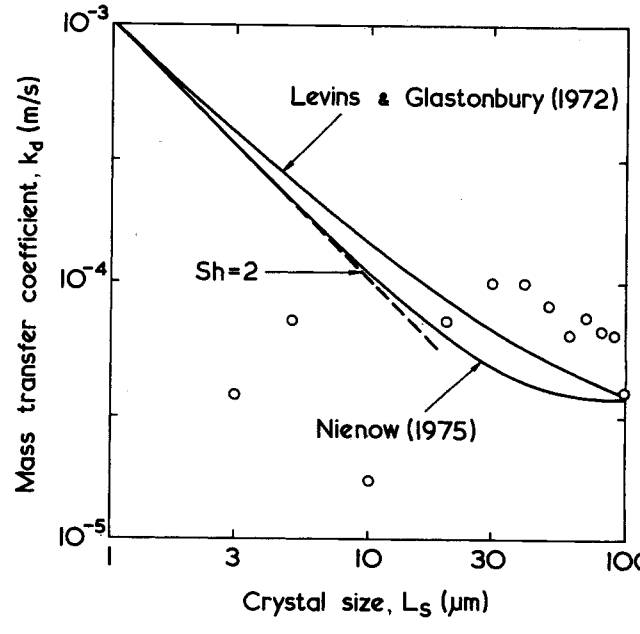

Fig. 7. Comparison of measured mass transfer coefficients with those predicted by various published correlations.

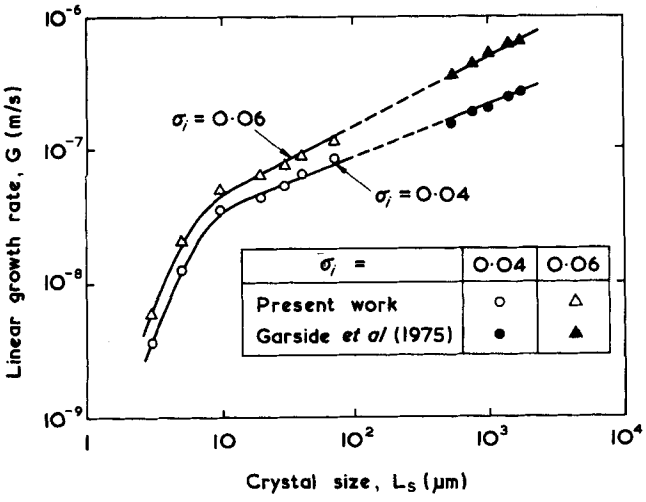

Fig. 8. Surface integration kinetics of potash alum at 30.0°C.

calculations are shown in Figure 8, where the growth rate is plotted against crystal size for two values of the supersaturation at the crystal/solution interface σ_i. The data, therefore, represent surface integration kinetics. Derived surface integration kinetics obtained in the present study are also included.

The data shown in Figure 8 cover a size range of almost three orders of magnitude, and, although no results are available in the range between about 100 and 500 μm, the two sets of data show a remarkable degree of consistency. The effect of size on the growth rate appears to depend somewhat on the supersaturation. For sizes greater than about 10 μm, the growth rate is proportional to $L^{0.38}$ for $\sigma_i = 0.04$ and to $L^{0.53}$ for $\sigma_i = 0.06$. There also appears to be a very sharp reduction in surface integration rate for crystals smaller than about 10 μm.

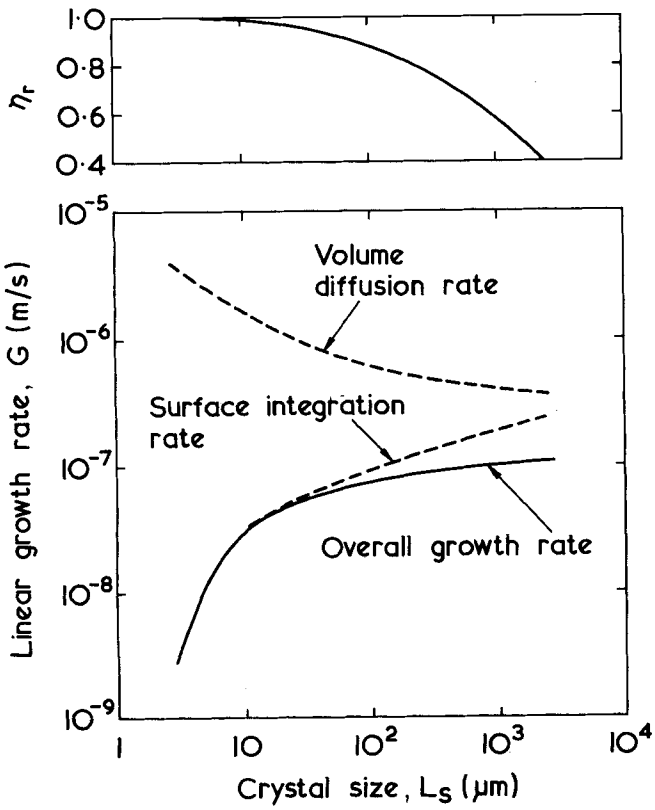

Fig. 9. Predicted overall growth rates in an agitated stirred-tank crystallizer (volume = 5 l, stirrer $Re = 10^5$. $\epsilon = 1 m^2/s^3$, $\sigma = 0.04$, that is, $(c - c^*) = 0.53 \times 10^{-2}$ kg hydrate/kg solution).

Somewhat similar results for potassium sulfate have been collated by White et al. (1974). Again, pronounced size dependent growth was apparent, although the potassium sulfate results represent overall kinetics. Furthermore, the growth rates were obtained from steady state CSDs in MSMPR crystallizers, and so the derived kinetics for small sizes would have been influenced by the occurrence of secondary nucleation.

DISCUSSION

Two aspects of the measured growth kinetics for small potash alum crystals are particularly notable; the surface integration kinetics are strongly size dependent and are also linear with respect to supersaturation.

The two independent sets of data shown in Figure 8 provide strong evidence that size dependent surface integration kinetics are exhibited by the potash alum/water system over a wide range of crystal size. Potassium sulfate (Garside et al., 1974) and nickel sulfate (Phillips and Epstein, 1974) are other salts for which similar behavior has been found, although in these cases only a comparatively narrow size range has been studied. Possible reasons for such behavior have been discussed by Garside et al. (1976). For example, the dislocation density may increase with increasing size as a result of mechanical stress, the incorporation of impurity atoms into the crystal lattice, or the occurrence of increasingly energetic crystal collisions. These increases in dislocation density would probably increase the strength of a step source (Bennema and Gilmer, 1973), as the stronger sources on a face eliminate the weaker sources.

Such a mechanism can be quantified in terms of the Burton, Cabrera, Frank (BCF) step model (Burton et al., 1951; Bennema and Gilmer, 1973) which predicts that the relation between linear face growth rate R and supersaturation σ is of the form

$$R = C \frac{\sigma^2}{\sigma_c} \tanh\left(\frac{\sigma_c}{\sigma}\right) \tag{13}$$

where

$$\sigma_c = 9.5\gamma' a/skTx_s \tag{14}$$

and s is a measure of the strength of the step sources. The relation between R and σ predicted by the BCF theory [Equation (13)] is parabolic ($R = C\sigma^2/\sigma_c$) for $\sigma << \sigma_c$ and linear ($R = C\sigma$) for $\sigma >> \sigma_c$. In practice, an experimentally determined relationship between R and σ would appear parabolic if σ were less than about $0.7\sigma_c$ and would appear linear for values of σ greater than about $1.5\sigma_c$ (Garside et al., 1975).

If the value of s increases with increasing crystal size, σ_c would decrease [Equation (14)], and the BCF equation would predict that the $R - \sigma$ relation would become more nearly linear for larger crystal sizes. On the other hand, small crystals, for which s is small and hence σ_c large, should exhibit parabolic $R - \sigma$ curves. Previous measurements of growth kinetics for large crystals, recently summarized by Garside et al. (1975), have all resulted in nonlinear $R - \sigma$ curves for the range of supersaturations used in the present work. Although accurate surface integration kinetics could not be obtained from all the published data, the values of n in Equation (11) appeared to be in the range between 1.5 and 2.5, while the estimated value of σ_c was about 0.1. The linear kinetics obtained in the present work imply that the value of σ_c for small crystals is smaller than for large crystals. Since the measured growth rates are linear for supersaturations σ greater than about 0.01, the maximum value of σ_c for small crystals (given by $\sigma_c \approx \sigma/1.5$) appears to be about 0.007. This is an order of magnitude smaller than the value estimated for

large crystals and implies that s is large for small crystals, which is in apparent conflict with the earlier suggestion.

A possible explanation for this discrepancy can be given in terms of the second linear law discussed by Bennema (1967), Bennema and Gilmer (1973), and Lewis (1974). This arises when the length of a grain boundary is large compared to the radius of a critical nucleus, and there are thus many ends of screw dislocations lying in the length of a grain boundary. A linear law is then obtained for which $R = C'\sigma$, with $0 < C' < C$. Bennema (1967) suggests that such a second linear law will not occur for large crystals because dominating groups of spirals (that is, groups of dislocations giving the highest production of steps per unit time) are probably always present. In agitated crystallizers, their presence is more likely owing to the many crystal collisions that must cocur.

Bennema and Gilmer (1973) also point out that several other mechanisms can destroy the linear relation that BCF assumed to exist between the density of steps emitted from a step source and the supersaturation, this being an essential feature of the BCF theory. It is perhaps relevant to note that Bennema (1966) obtained linear $R - \sigma$ curves for potash alum crystals grown at very low supersaturations ($10^{-4} < \sigma < 10^{-2}$) which again were in apparent conflict with growth rates at higher supersaturations.

Although the mechanism of size dependent growth discussed here is speculative at this stage, the occurrence of size dependent growth has important implications for the derivation of crystallization kinetics from crystal size distributions. The overall growth rate in a crystallizer will be determined by the total series resistance offered by the volume diffusion and surface integration steps. Figure 9 shows the derived surface integration kinetics for $\sigma = 0.04$ (as previously shown in Figure 8), together with the predicted overall growth rate in a 5 l agitated vessel as used by Jančić (1976). This crystallizer is taken as typical of those used for laboratory MSMPR studies. The mass transfer coefficients (and hence the volume diffusion resistance) used for this prediction were calculated from the correlation of Levins and Glastonbury (1972), the appropriate parameters being indicated in Figure 9.

It is clear that in this case the overall growth rate becomes increasingly controlled by the volume diffusion step as the crystal size increases. At larger sizes, the increasing volume diffusion resistance begins to counteract the increasing surface integration kinetics, and above about 500 μm the overall growth rate is almost independent of size. This increasing volume diffusion resistance can be quantified by the value of the surface integration effectiveness factor η_r (Garside, 1971), the value of which is defined by

$$\eta_r = \frac{\text{measured overall growth rate}}{\text{growth rate that would be obtained if the crystal surface were exposed to conditions in the bulk solution}} \qquad (15)$$

η_r becomes significantly less than unity for sizes greater than about 100 μm, while for small crystals the overall kinetics are determined solely by the surface integration kinetics. It thus seems likely that the overall growth rates of small crystals (less than about 100 μm) will always be very similar to the surface integration kinetics, the diffusion resistance being small in this range and the overall growth rate being essentially independent of the hydrodynamic conditions. Comparison of growth rates in the small size range as measured by different authors should therefore be less affected by uncertainties in defining the hydrodynamics of the growth environment. Further, there should be less uncertainty in predicting growth rates in this size range for different hydrodynamic systems and scales of operation.

The results shown in Figure 9 illustrate that overall crystal growth rates can be strongly size dependent for the size ranges into which secondary nuclei are born. The importance of measuring growth kinetics independently of nucleation kinetics before meaningful secondary nucleation rates can be calculated from steady state size distributions in MSMPR crystallizers is thus emphasized.

It is important to emphasize that the growth phenomena reported here for potash alum may not be typical of all systems. Indeed, there is some recent evidence that the growth rate of many small crystals of both pentaerythritol (Bujac, 1976) and sodium chloride (van't Land and Wienk, 1976) is immeasurably small and other evidence suggesting that magnesium sulfate exhibits size independent growth rates for crystals larger than about 8 μm (Sikdar and Randolph, 1976).

NOTATION

a = shortest distance between growth units
b = constant in Equation (5)
c = solution concentration (kg hydrate/kg solution)
c^* = saturation concentration (kg hydrate/kg solution)
C = parameter in BCF growth equation [Equation (13)]
C' = constant in the second linear law
d = stirrer diameter
f_s = surface shape factor
f_v = volume shape factor
g = constant in Equation (6)
G = linear growth rate ($= dL/dt$ in general and dL_s/dt for potash alum)
G_D = linear dissolution rate ($= -dL/dt$ in general and $-dL_s/dt$ for potash alum)
G_o = growth rate of nuclei [Equation (5)]
k = Boltzmann constant
k_d = mass transfer coefficient (m/s)
k_r = growth rate coefficient for surface integration kinetics [Equation (11)]
K_G = overall growth rate coefficient [Equation (4)]
K_{Go} = overall nuclei growth rate coefficient [Equation (6)]
L = crystal size
L_c = Coulter counter channel size
L_s = length of an edge of a potash alum octahedral crystal
n = exponent of supersaturation for surface integration kinetics [Equation (11)]
N = cumulative number of crystals
N_s = stirrer rotational speed (rev/s)
R = linear face growth rate
R_D = dissolution rate expressed as a mass flux (kg/m^2 s)
s = strength of a step source
s_c = surface area of a single crystal
t = time
T = absolute temperature
v_c = volume of a single crystal
x_s = mean diffusion distance of an adsorbed growth unit on the crystal surface

Greek Letters

γ = constant in Equation (5)
γ' = edge free energy of a growth unit in a step
ϵ = power dissipation per unit mass (m^2/s^3)
μ = solution viscosity
η_r = surface integration effectiveness factor [Equation (15)]
ρ = solution concentration (kg hydrate/m^3 solution)
ρ^* = saturation concentration (kg hydrate/m^3 solution)
ρ_c = crystal density
ρ_i = solution concentration at the crystal/solution in-

terface (kg hydrate/m³ solution)
ρ_s = solution density
σ = supersaturation [$= (\rho - \rho^*)/\rho^*$]
σ_c = parameter in BCF growth equation [Equation (14)]
σ_i = supersaturation at the crystal/solution interface [$= (\rho_i - \rho^*)/\rho^*$]

LITERATURE CITED

ASTM Special Technical Publication No. 331, *Manual of Hydrocarbon Analysis,"* 1 ed., Philadelphia, Pennsylvania (1963).
Abegg, C. F., J. D. Stevens, and M. A. Larson, *AIChE J.*, **14**, 118 (1968).
Bennema, P., *Phys. Status Solidi*, **17**, 563 (1966).
———, *J. Crystal Growth*, **1**, 278 (1967).
———, and G. H. Gilmer, in *Crystal Growth: An Introduction*, P. Hartman, ed., North Holland, Amsterdam (1973).
Bujac, P. D. B., in *Industr'al Crystallization*, J. W. Mullin, ed., p. 23, Plenum Press, New York (1976).
Burton, W. K., N. Cabrera, and F. C. Frank, *Phil. Trans. Royal Soc.*, **243**, 299 (1951).
Garside, J., *Chem. Eng. Sci.*, **26**, 1425 (1971).
———, J. W. Mullin, and S. N. Das, *Ind. Eng. Chem., Fundamentals*, **13**, 299 (1974).
Garside, J., R. Janssen-Van Rosmalen, and P. Bennema, *J. Crystal Growth*, **29**, 353 (1975).
Garside, J., V. R. Phillips, and M. B. Shah, *Ind. Eng. Chem. Fundamentals*, **15**, 230 (1976).
Jančić, S. J., and J. Garside, *Chem. Eng. Sci.*, **30**, 1299 (1975).
———, in *Industrial Crystallization*, J. W. Mullin, ed., p. 365, Plenum Press, New York (1976).
Jančić, S. J., Ph.D. thesis, Univ. London, England (1976).
Levins, D. M., and J. R. Glastonbury, *Trans. Inst. Chem. Engrs.*, **50**, 132 (1972).
Lewis, B., *J. Crystal Growth*, **21**, 29, 40 (1974).
Misra, C., and E. T. White, *Chem. Eng. Progr. Symposium Ser. No. 110*, **67**, 53 (1971).
Mullin, J. W., J. Garside, and R. Unahabhoka, *J. Appl. Chem.*, **15**, 502 (1965).
Mullin, J. W., and J. Garside, *Trans. Inst. Chem. Engrs*, **45**, T291 (1967).
Nagata, S., and N. Nishikawa, *Proc. First Pacific Chem. Eng. Congr.*, Soc. Chem. Eng. (Japan) and AIChE, Kyoto (Oct. 10-14, 1972).
Nienow, A. W., and D. Miles, *Ind. Eng. Chem. Process Design Develop.*, **10**, 41 (1971).
Nienow, A. W., *Chem. Eng. J.*, **9**, 153 (1975).
Phillips, V. R., and N. Epstein, *AIChE J.*, **20**, 678 (1974).
Randolph, A. D., and M. D. Cise, *ibid.*, **18**, 798 (1972).
Sikdar, S. K., and A. D. Randolph, *ibid.*, **22**, 110 (1976).
van't Land, C. M. and B. G. Wienk, in *Industrial Crystallization*, J. W. Mullin, ed., p. 51, Plenum Press, New York (1976).
White, E. T., L. L. Bendig, and M. A. Larson, "The Effect of Size on the Growth Rates of K_2SO_4 Crystals," Paper presented at the 67th Annual AIChE Meeting, Washington, D. C. (1974).
Youngquist, G. R., and A. D. Randolph, *AIChE J.*, **18**, 421 (1972).

Manuscript received March 23, 1976; revision received May 7 and accepted May 10, 1976.

A New Tracer Method for Determination of Liquid-Solid Contacting Efficiency in Trickle-Bed Reactors

J. G. SCHWARTZ
ERIC WEGER
and
M. P. DUDUKOVIC

Chemical Reaction Engineering Laboratory
Department of Chemical Engineering
Washington University
St. Louis, Missouri 63130

A new tracer technique is reported for the determination of liquid-solid contacting efficiency and liquid holdup in trickle beds packed with small alumina particles. Holdup was a function of liquid mass velocity for both porous and nonporous packing. Contacting efficiency remained uniform at a level of 65%.

SCOPE

A trickle bed consists of a fixed bed of catalyst particles with liquid, containing one or more of the reactants, trickling through the bed. A gas, containing the other reactant(s), is simultaneously passed through the bed. The major problems in the scale-up of trickle beds have been the difficulties in predicting the extent and effect on reactor performance of contacting between the solid catalyst and liquid, of mass and heat transfer within and to the catalyst particles, and of liquid backmixing. The progress to date on research in these areas was recently summarized in an excellent review paper (Satterfield, 1975).

Our objectives were to develop a method for evaluation of liquid-solid contacting which would be applicable to both porous and nonporous packing and to compare the experimental results obtained with the predictions of the available correlations over a range of liquid flow rates. A new two-tracer method was developed for this purpose. Hexane was used as the liquid phase and helium as the gas. Heptane was employed as the nonadsorbable tracer, and benzene and naphthalene were used as the adsorbable ones. The theory of chromatography was used to relate the first moments of the residence time distributions of the two types of tracers to liquid holdup and contacting efficiency.

J. G. Schwartz is with the Amoco Oil Company, Amoco Research Center, Naperville, Illinois.